Title

Associations among locus coeruleus catecholamines, tau pathology, and memory in aging.

Journal

Neuropsychopharmacology : official publication of the American College of Neuropsychopharmacology, 47(5)

ISSN

0893-133X

Authors

Ciampa, Claire J
Parent, Jourdan H
Harrison, Theresa M
et al.

Publication Date

2022-04-01

DOI

10.1038/s41386-022-01269-6

Peer reviewed

American College of Neuropsychopharmacology

ARTICLE

Check for updates

Associations among locus coeruleus catecholamines, tau pathology, and memory in aging

Claire J. Ciampa[1,8], Jourdan H. Parent[1,8], Theresa M. Harrison[2], Rebekah M. Fain[1], Matthew J. Betts[3,4,5], Anne Maass[4], Joseph R. Winer[2], Suzanne L. Baker[6], Mustafa Janabi[6], Daniella J. Furman[2,7], Mark D'Esposito[2], William J. Jagust[2,6] and Anne S. Berry[1,6]✉

The locus coeruleus (LC) is the brain's major source of the neuromodulator norepinephrine, and is also profoundly vulnerable to the development of Alzheimer's disease (AD)-related tau pathology. Norepinephrine plays a role in neuroprotective functions that may reduce AD progression, and also underlies optimal memory performance. Successful maintenance of LC neurochemical function represents a candidate mechanism of protection against the propagation of AD-related pathology and may facilitate the preservation of memory performance despite pathology. Using [^{18}F]Fluoro-m-tyrosine ([^{18}F]FMT) PET imaging to measure catecholamine synthesis capacity in LC regions of interest, we examined relationships among LC neurochemical function, AD-related pathology, and memory performance in cognitively normal older adults ($n = 49$). Participants underwent [^{11}C]Pittsburgh compound B and [^{18}F]Flortaucipir PET to quantify β-amyloid ($n = 49$) and tau burden ($n = 42$) respectively. In individuals with substantial β-amyloid, higher LC [^{18}F]FMT net tracer influx (Ki_{vis}) was associated with lower temporal tau. Longitudinal tau-PET analyses in a subset of our sample ($n = 30$) support these findings to reveal reduced temporal tau accumulation in the context of higher LC [^{18}F]FMT Ki_{vis}. Higher LC catecholamine synthesis capacity was positively correlated with self-reported cognitive engagement and physical activity across the lifespan, established predictors of successful aging measured with the Lifetime Experiences Questionnaire. LC catecholamine synthesis capacity moderated tau's negative effect on memory, such that higher LC catecholamine synthesis capacity was associated with better-than-expected memory performance given an individual's tau burden. These PET findings provide insight into the neurochemical mechanisms of AD vulnerability and cognitive resilience in the living human brain.

Neuropsychopharmacology (2022) 47:1106–1113; https://doi.org/10.1038/s41386-022-01269-6

INTRODUCTION

Models of the pathogenesis of Alzheimer's disease (AD) suggest abnormal tau spreads from the locus coeruleus (LC) to connected temporal lobe regions [1]. The LC is the brain's primary source of norepinephrine, a neuromodulator that has been linked to a striking number of neuroprotective functions including reduction of inflammation [2] and promotion of neurotrophic factors [3]. Despite these neuroprotective functions, elevated norepinephrine metabolites are associated with greater tau pathology and cognitive impairment in AD [4–7], and may promote the cleavage of tau into aggregation and propagation-prone forms [8]. Given the therapeutic targeting of the LC-norepinephrine system in AD, basic research is needed to establish relationships between endogenous LC neurochemical function and tau pathology in vivo.

The central role of the LC in AD has made it a target for neuroimaging biomarker development. These efforts have concentrated on specialized magnetic resonance (MR) imaging sequences for which hyperintense MR signal is interpreted to reflect greater LC structural integrity (i.e., cell density) [9]. Greater LC structural integrity has been linked with indicators of successful aging including greater cortical thickness [10] and cognitive reserve [11, 12]. Research associating LC neuroimaging measures with the development of AD-related pathology in vivo is in its infancy. Initial studies find reduced LC integrity is associated with elevated cerebrospinal fluid (CSF) measures of β-amyloid in AD [13], and higher brain tau measured with positron emission tomography (PET) in aging [14] and autosomal dominant AD [15]. Together, these studies reveal LC to reflect neurobiological aging trajectories, which may be particularly valuable if applied to early detection of disease vulnerability.

The LC-norepinephrine system is critical for optimal cognitive performance [16, 17] including episodic memory [15, 18–20]. In mouse models of AD, LC lesions exacerbate memory impairments [21, 22]. This suggests the negative effect of AD-related pathology on episodic memory in humans may be heightened by accompanying disruption of the LC-norepinephrine system. Conversely, the successful maintenance of LC function despite

[1]Department of Psychology, Brandeis University, Waltham, MA 02453, USA. [2]Helen Wills Neuroscience Institute, University of California, Berkeley, Berkeley, CA 94720, USA. [3]Institute of Cognitive Neurology and Dementia Research, Otto von Guericke University, Magdeburg 39106, Germany. [4]Deutsches Zentrum für Neurodegenerative Erkrankungen, Magdeburg 39120, Germany. [5]Center for Behavioral Brain Sciences, University of Magdeburg, Magdeburg, Germany. [6]Lawrence Berkeley National Laboratory, Berkeley, CA 94720, USA. [7]University of California, San Francisco, San Francisco, CA 94143, USA. [8]These authors contributed equally: Claire J. Ciampa and Jourdan H. Parent. ✉email: anneberry@brandeis.edu

Received: 22 September 2021 Revised: 16 November 2021 Accepted: 4 January 2022
Published online: 15 January 2022

AD pathology may support the relative preservation of memory, representing a neurobiological mechanism of cognitive resilience [23–26].

While methods development for structural LC imaging is accelerating, these methods do not provide direct insight into LC neurochemical function. We pursued LC imaging with the irreversible PET tracer [^{18}F]Fluoro-m-tyrosine ([^{18}F]FMT). [^{18}F]FMT is a substrate for aromatic amino acid decarboxylase (AADC) and is a measure of monoamine synthesis capacity. [^{18}F]FMT PET can be used to measure synthesis capacity of catecholamines norepinephrine and dopamine in the LC [27], catecholamine dopamine in the midbrain (ventral tegmental area/substantia nigra; VTA/SN) and striatum, and monoamine serotonin in the raphe nuclei. This study in cognitively normal older adults takes the first steps towards defining fundamental relationships among LC neurochemical function, AD-related tau pathology and episodic memory in aging. Parallel analyses in raphe, midbrain and striatum illustrate the specificity of these relationships.

MATERIALS AND METHODS

Study design

Forty-nine older adults (mean age = 77.18, standard deviation (SD) = 5.80, range = 62–85, 29 female; mean years of education = 16.61, SD = 2.04, range = 12–20) are included and underwent [^{18}F]FMT PET, [^{11}C]Pittsburgh compound B PET ([^{11}C]PiB) and memory testing. Of these participants, 42 underwent [^{18}F]Flortaucipir PET. Participants were part of the Berkeley Aging Cohort Study, scored at least 25 on the Mini-Mental State Exam (mean = 28.69, SD = 1.26), and were characterized as cognitively normal [28]. Participants did not have a neurological, psychological, or psychiatric disorder, and did not take medication affecting cognition. The University of California, Berkeley, and Lawrence Berkeley National Laboratory Institutional Review Boards approved the study. Informed consent was obtained from all participants.

Structural MRI

Whole-brain images were acquired using a Siemens 3 T Trio Tim and 32-channel coil. T1-weighted volumetric magnetization prepared rapid gradient echo image sequence was acquired (TR = 2,3000 ms, TE = 2.98 ms, matrix = 256 × 256; FOV = 256; sagittal plane; 1 x 1 x 1 mm; 160 slices). Scans were segmented using FreeSurfer 5.3.0 (http://surfer.nmr.mgh.harvard.edu/). Structural templates were generated in MNI space using Statistical Parametric Mapping software's DARTEL (SPM12; Wellcome Trust Center for Neuroimaging, London, UK).

[^{18}F]FMT PET

Participants underwent [^{18}F]FMT PET scanning using a Siemens Biograph Truepoint 6 PET/CT and previously described methods [29, 30]. Supplemental Methods describe the strengths and limitations of [^{18}F]FMT. Dynamic acquisition frames were obtained over 90 min in 3D mode. Frames were realigned, coregistered, and resliced to structural T1s [30]. Graphical analysis using a Patlak plot [31] was performed with a reference region approach rather than arterial plasma input function. Whole-brain images were generated using primary visual cortex (lingual gyrus and cuneus) reference region and PET frames corresponding to 25 to 90 min [32]. Whole-brain Ki_{vis} images were normalized to the DARTEL template. Ki_{vis} represents the amount of tracer accumulated in the brain relative to the visual cortex reference region. These images are comparable to Ki images obtained using an arterial plasma input function, but are scaled to the volume of tracer distribution in the reference region. However, this approach assumes minimal specific binding in visual cortex, and specific binding that does not vary substantially across individuals. It is also important to note that assuming the system is in equilibrium, Ki_{vis} is affected by K_1, [^{18}F]FMT's rate constant from blood to tissue (product of perfusion and extraction). Therefore, it is possible that reduced delivery to the LC would result in lower LC Ki_{vis}. Future research measuring blood flow to LC will be necessary to determine the extent to which [^{18}F]FMT Ki_{vis} is confounded by individual differences in K_1.

Primary [^{18}F]FMT analyses relied on LC regions of interest (ROIs) derived from an LC meta-ROI developed by Dahl and colleagues [15] based on previously published MR templates [18, 33–36]. Accurate coregistration (nearest-neighbor interpolation) was confirmed in Mango (https://www.nitrc.org/projects/mango/). To accommodate PET resolution, we smoothed the MR-derived LC ROI (4 mm FWHM) and thresholded (>0.147) to generate a mask of 479 1 x 1 x 1 mm voxels, that is approximately 6x the size of the original ROI (ROI available: https://neurovault.org/images/442231/). Given concerns about LC's proximity to the raphe, we report parallel [^{18}F]FMT Ki_{vis} analyses using dorsal and median raphe ROIs [37]. For completeness, we report results for VTA/SN, and striatum ROIs. Statistical analyses appear in main text, though see the Supplement for supporting Methods and Figures.

Though previous studies report PET signal in LC [38–47], for transparency, we display whole-brain voxel-wise analyses to support the use of [^{18}F]FMT Ki_{vis} to measure brainstem signal. In the Supplement, we report voxel-wise regression analyses with LC [^{18}F]FMT Ki_{vis} as the independent variable to illustrate the degree to which [^{18}F]FMT Ki_{vis} measured in the LC ROI covaried with [^{18}F]FMT Ki_{vis} throughout the brain, giving insight into the regional specificity of signal patterns in the brainstem (Figure S1).

[^{18}F]Flortaucipir and [^{11}C]PiB PET

All participants underwent [^{11}C]PiB scanning to assess β-amyloid status and a subset underwent [^{18}F]Flortaucipir scanning (n = 42) to measure tau pathology within 3 years of their [^{18}F]FMT scan. The median time difference between [^{18}F]FMT and [^{11}C]PiB scans was 328 days (SD = 245; range = 14–966). The median time difference between [^{18}F]FMT and [^{18}F] Flortaucipir scanning was 176 days (SD = 236; range = 9–945). A subset of participants (n = 30; 10 [^{11}C]PiB positive, 20 [^{11}C]PiB negative) had multiple [^{18}F]Flortaucipir scans (average number of timepoints per participant = 2.5; total number of [^{18}F]Flortaucipir scans = 74).

A detailed description of [^{11}C]PiB and [^{18}F]Flortaucipir acquisition has been published previously [48]. [^{11}C]PiB distribution volume ratio (DVR) images were generated with Logan graphical analysis on frames corresponding to 35–90 min post-injection using cerebellar gray matter reference region [49]. β-amyloid-positivity was based on global cortical [^{11}C]PiB distribution volume ratio 1.065 or greater [50, 51].

[^{18}F]Flortaucipir SUVR images were generated from frames corresponding to 80–100 min post-injection using inferior cerebellar gray matter reference. SUVR images were partial volume corrected as previously described [52]. [^{18}F]Flortaucipir SUVR was measured within a previously established PET meta-ROI comprised of tau-vulnerable regions [53]. The tau PET meta-ROI was formed from a voxel-weighted average of the mean uptake in entorhinal, amygdala, parahippocampal, fusiform, inferior temporal, and middle temporal ROIs. Due to the relatively small sample (n = 30), longitudinal [^{18}F]Flortaucipir analyses are considered preliminary. Longitudinal [^{18}F]Flortaucipir scans were processed with a longitudinal pipeline and white matter reference region as previously described [54]. To measure change in [^{18}F]Flortaucipir, the partial volume corrected SUVR at each time point was entered into linear mixed effects models with random effects for participant intercept and slope.

Neuropsychological testing

Participants underwent neuropsychological testing (median time difference from [^{18}F]FMT = 144 days; SD = 101; range = 6–420). A composite memory measure was calculated using each participant's California Verbal Learning Test-II [55] performance. Based on previous research demonstrating relationships between the LC-norepinephrine system and verbal learning and memory measures [7, 15, 18, 20], the composite was comprised of free recall performance during learning trials 1-5 and free recall following the long delay (Supplemental Methods).

To investigate the role of higher LC catecholamine synthesis capacity as a mechanism of cognitive resilience and reserve, we explored its relationship with a proxy measure of cognitive reserve: cognitive engagement across the lifespan. We measured Lifetime Experiences Questionnaire (LEQ) [56] total score, which assesses complex mental activity and physical activity across the lifetime. We excluded LEQ data from two participants due to incomplete responding, and misinterpretation of instructions (some additive rather than discrete estimations across years).

Statistical testing

Analyses were performed using IBM SPSS v27. Multiple linear regression models included age, sex, and years of education as covariates. We report regression models with and without [^{18}F]FMT Ki_{vis} and [^{11}C]PiB interaction terms given ambiguity as to whether tau-pathologic processes involving

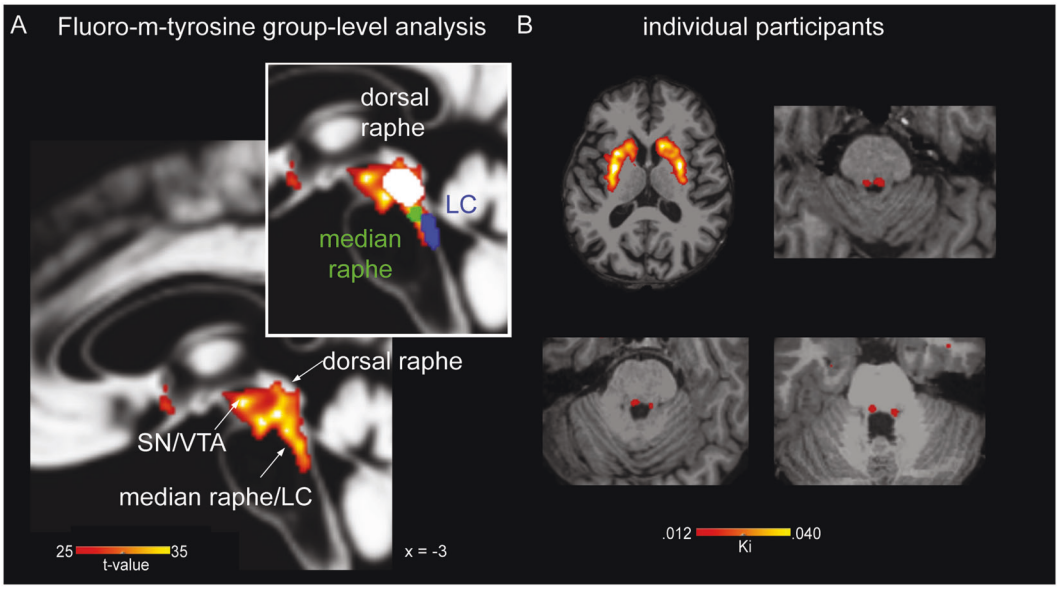

Fig. 1 Locus coeruleus-related [^{18}F]Fluoro-m-tyrosine signal ([^{18}F]FMT). A Whole-brain analyses of [^{18}F]FMT data for all subjects ($n = 49$) reveals significant PET signal in regions consistent with the substantia nigra/ventral tegmental area (SN/VTA), raphe nuclei, and locus coeruleus (LC) (one-sample t-test; voxel-wise threshold $p < 1 \times 10^{-16}$). Inset displays overlaid regions of interest (ROIs). Results are overlaid on the older adults' study-specific DARTEL template. **B** [^{18}F]FMT Ki_{vis} scans overlaid on structural T1 scans in native space for 3 participants.

the LC are AD-related or age-related [57, 58]. For interaction models, independent variables were mean-centered. Years of education was excluded for regression models involving LEQ, as education contributes to this measure. Bootstrap 95% confidence intervals were calculated using the Robust Correlation Toolbox in MATLAB 2020b [59]. Post hoc testing of the moderation analysis testing a role of LC [^{18}F]FMT Ki_{vis} in cognitive resilience was performed using PROCESS v4.0 [60].

RESULTS

Visualization of LC with [^{18}F]FMT PET

Whole-brain voxel-wise analysis of [^{18}F]FMT Ki_{vis} maps revealed a highly significant contiguous midline cluster in the midbrain and brainstem with peaks consistent with the VTA/SN, LC, and raphe nuclei (Fig. 1A; Table S1A). While brainstem signal was greatest in midline regions consistent with the raphe, [^{18}F]FMT Ki_{vis} signal in lateral regions consistent with LC is clear in individual participant scans at thresholds typically used to visualize [^{18}F]FMT binding in the striatum (Fig. 1B).

LC catecholamine synthesis capacity is associated with tau burden in Aβ + participants

[^{18}F]FMT Ki_{vis} within the LC ROI did not differ between [^{11}C]PiB positive ($n = 14$) and negative participants ($n = 35$; $t(47) = 0.73$, $p = 0.47$). [^{18}F]Flortaucipir SUVR in tau vulnerable regions (Fig. 2A), was higher in [^{11}C]PiB positive older adults (Levene's test for equality of variances $p = 0.001$; $t(12) = 2.65$, $p = 0.02$, $d = 1.29$, 95% CI [0.56, 2.01]; $n = 12$ [^{11}C]PiB positive, $n = 30$ [^{11}C]PiB negative; Fig. 2B), replicating previous reports [53]. LC [^{18}F]FMT Ki_{vis} was not associated with [^{18}F]Flortaucipir SUVR in a model adjusting for age, sex and years of education (Table 1A). A model including [^{11}C]PiB status and LC [^{18}F]FMT by [^{11}C]PiB interaction revealed a significant interaction (Table 1A; Fig. 2C). Higher LC [^{18}F]FMT Ki_{vis} was related to lower [^{18}F]Flortaucipir SUVR in [^{11}C]PiB positive ($r = -0.60$ [−0.92 −0.03], $p = 0.04$) but not [^{11}C]PiB negative participants ($r = 0.12$ [−0.39 0.40], $p = 0.54$). Adjusting for days between [^{18}F]Flortaucipir and [^{18}F]FMT scan did not affect the interaction (beta = −0.48, $p = 0.002$). [^{11}C]PiB negative and positive groups did not differ in the time between [^{18}F]Flortaucipir and [^{18}F]FMT scans ($t(41) = 0.39$, $p = 0.35$).

Suggesting our findings are specific to LC [^{18}F]FMT Ki_{vis}, analyses of raphe [^{18}F]FMT Ki_{vis} found no relationship with [^{18}F]Flortaucipir SUVR (dorsal: beta = 0.22, $p = 0.20$; median: beta = 0.25, $p = 0.15$; Fig. S2) and no interactions with [^{11}C]PiB status (dorsal: beta = 0.07, $p = 0.67$; median: beta = −0.01, $p = 0.93$). Similarly, analyses of midbrain (VTA/SN) and striatal ROIs found no relationship with [^{18}F]Flortaucipir SUVR (midbrain: beta = 0.001, $p = 0.99$; striatum: beta = 0.11, $p = 0.49$; Fig. S2) and no interactions with [^{11}C]PiB status (midbrain: beta = 0.11, $p = 0.47$; striatum: beta = 0.06, $p = 0.70$).

Summary Fig. 2D depicts longitudinal [^{18}F]Flortaucipir acquisition timepoints relative to each participant's [^{18}F]FMT scan. There was not a significant difference in [^{18}F]Flortaucipir slopes for [^{11}C]PiB positive ($n = 10$) relative to negative participants ($n = 20$; Levene's test for equality of variances $p = 0.02$; $t(10) = 1.60$, $p = 0.14$; Fig. 2E). Higher [^{18}F]Flortaucipir slope was associated with lower LC [^{18}F]FMT Ki_{vis} for a model adjusting for age, sex, years of education and [^{11}C]PiB status (Table 1B). Consistent with cross-sectional analyses, there was a significant interaction between [^{18}F]FMT Ki_{vis} and [^{11}C]PiB status suggesting that relationships between LC [^{18}F]FMT Ki_{vis} and increasing [^{18}F]Flortaucipir are stronger in [^{11}C]PiB positive participants, though the correlation was only marginal for [^{11}C]PiB positive participants alone (Table 1B; Fig. 2F; [^{11}C]PiB positive: $r = -0.59$ [−0.78, 0.35], $p = 0.07$; [^{11}C]PiB negative: $r = -0.35$ [−0.75 0.30], $p = 0.13$). We do not interpret the lack of significance of this relationship strongly given the limited sample size (10 [^{11}C]PiB positive). The significant [^{18}F]FMT Ki_{vis} * [^{11}C]PiB status interaction was not affected by the addition of a covariate adjusting for relative timing of [^{18}F]Flortaucipir scans before or after the [^{18}F]FMT Ki_{vis} scan (interaction beta = −0.52, $p = 0.04$; Supplementary Methods).

These relationships were not evident for analyses of raphe [^{18}F]FMT Ki_{vis}, midbrain or striatum. In contrast to LC [^{18}F]FMT Ki_{vis} findings, no other ROI predicted [^{18}F]Flortaucipir slope for models including [^{11}C]PiB status (dorsal raphe: beta = 0.15, $p = 0.55$ median raphe: beta = 0.19, $p = 0.42$; midbrain: beta = 0.06, $p = 0.77$; striatum: beta = −0.04, $p = 0.84$; Fig. S2). Further, there were no interactions with [^{11}C]PiB status (dorsal: beta = 0.06, $p = 0.77$; median: beta = 0.11, $p = 0.59$; midbrain: beta = −0.14, $p = 0.49$; striatum: beta = −0.09, $p = 0.65$).

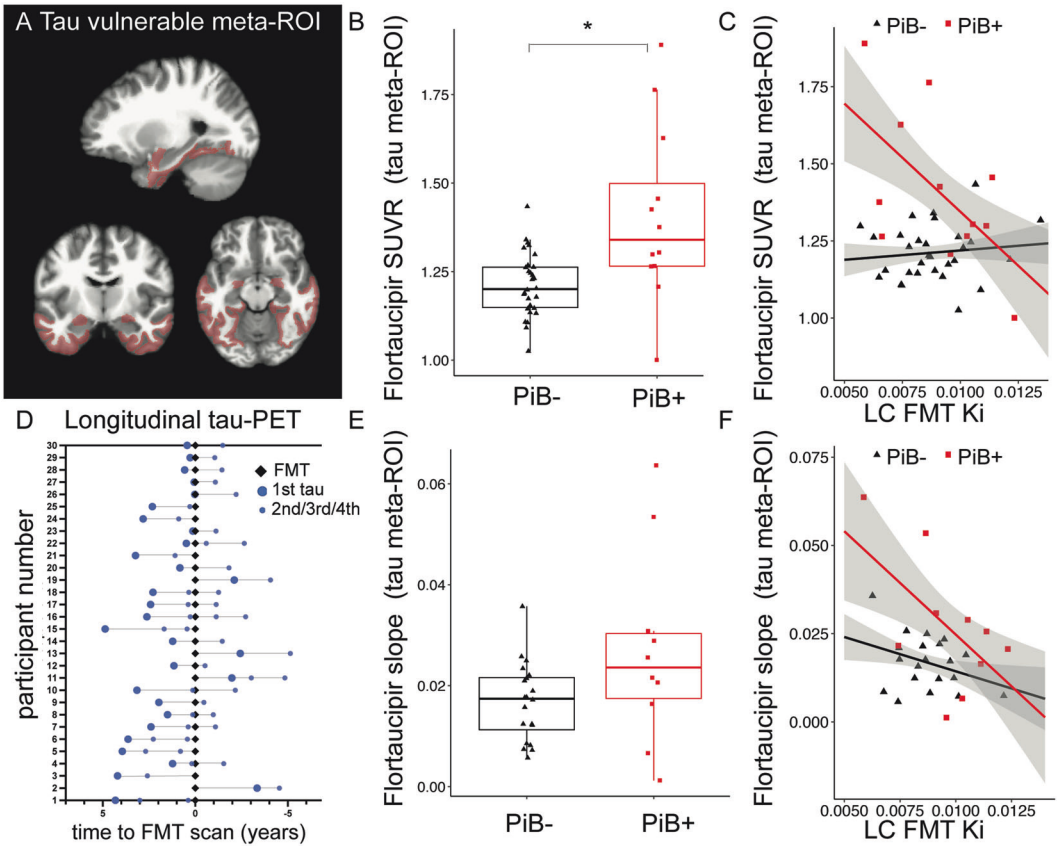

Fig. 2 Relationship between [^{18}F]Fluoro-m-tyrosine ([^{18}F]FMT) Ki and [^{18}F]Flortaucipir SUVR. A [^{18}F]Flortaucipir SUVR was measured in a voxel-weighted meta-ROI. **B** [^{18}F]Flortaucipir SUVR was related to β-amyloid status as defined by [^{11}C]Pittsburgh compound B (PiB). [^{18}F]Flortaucipir SUVR was significantly higher in [^{11}C]PiB positive subjects. **C** A regression model with [^{18}F]Flortaucipir as the dependent variable revealed an interaction between locus coeruleus (LC) [^{18}F]FMT Ki_{vis} and [^{11}C]PiB status. **D** This schematic displays the temporal relationship between [^{18}F]FMT PET and longitudinal [^{18}F]Flortaucipir PET scans. **E** There was not a difference in [^{18}F]Flortaucipir slope between [^{11}C]PiB positive and negative individuals. **F** A regression model with [^{18}F]Flortaucipir slope derived from the linear mixed effect model as the dependent variable revealed an interaction between LC [^{18}F]FMT Ki_{vis} and [^{11}C]PiB status.

Tau, LC catecholamine synthesis capacity, and memory

LC [^{18}F]FMT Ki_{vis} did not predict CVLT memory composite (beta = 0.07, $p = 0.64$; Fig. 3A). A model including [^{11}C]PiB status revealed a relationship between [^{11}C]PiB status and memory (beta = −0.31, $p = 0.03$; $n = 12$ [^{11}C]PiB positive, $n = 30$ [^{11}C]PiB negative), but no interaction between LC [^{18}F]FMT Ki_{vis} and [^{11}C]PiB (beta = 0.10, $p = 0.53$). Consistent with previous reports [61], higher [^{18}F]Flortaucipir SUVR predicted lower memory (beta = −0.33, $p = 0.04$; Fig. 3B). This relationship was strongest for [^{11}C]PiB positive participants ([^{18}F]Flortaucipir * [^{11}C]PiB; beta = −0.57, $p = 0.02$).

While LC [^{18}F]FMT Ki_{vis} was not associated with better memory overall, we examined whether higher LC [^{18}F]FMT Ki_{vis} was associated with better-than-expected memory given an individual's tau burden. In line with the framework of resilience, we tested for the critical interaction between LC [^{18}F]FMT Ki_{vis} and [^{18}F]Flortaucipir SUVR [23, 24]:

Memory ~ [^{18}F]Flortaucipir SUVR + LC [^{18}F]FMT Ki_{vis} + **[^{18}F]Flortaucipir SUVR * LC [^{18}F]FMT Ki_{vis}** + age + sex + years of education.

This model revealed a significant interaction between [^{18}F]Flortaucipir SUVR and LC [^{18}F]FMT Ki_{vis} (beta = 0.37, $p = 0.04$). Addition of [^{11}C]PiB status to the model did not change these results (beta = 0.37, $p = 0.04$). To visualize the [^{18}F]Flortaucipir * [^{18}F]FMT Ki_{vis} interaction, the unstandardized simple slopes were tested for low (−1 SD), moderate, and high (+1 SD) levels of LC [^{18}F]FMT Ki_{vis} [60]. Variation in the slopes of the regression lines with varying levels of [^{18}F]FMT Ki_{vis} show results consistent with a role of [^{18}F]FMT Ki_{vis} in cognitive resilience. The negative impact of tau pathology on memory is only evident for individuals with low and medium levels of LC [^{18}F]FMT Ki_{vis}. At high levels of LC [^{18}F]FMT Ki_{vis}, this relationship was not apparent (Fig. 3C).

Analyses substituting raphe, midbrain, and striatal ROIs found no relationships with memory (dorsal: beta = 0.02, $p = 0.91$; median: beta = 0.01, $p = 0.94$; midbrain: beta = 0.10, $p = 0.51$; striatum: beta = -0.06, $p = 0.68$; Figure S3) or interactions with [^{18}F]Flortaucipir SUVR (dorsal: beta = -0.21, $p = 0.30$; median: beta = −0.19, $p = 0.31$; midbrain: beta = 0.11, $p = 0.52$; striatum: beta = −0.08, $p = 0.62$).

LC catecholamine synthesis capacity and lifespan cognitive engagement

Evidence of a moderating effect of LC [^{18}F]FMT Ki_{vis} on tau's negative relationship with memory is consistent with the interpretation that higher LC catecholamine synthesis represents a mechanism of cognitive resilience [24]. However, there were relatively few participants with high levels of [^{18}F]Flortaucipir SUVR, leading us to interpret this interaction with caution. Next, we tested LC [^{18}F]FMT Ki_{vis}'s relationship with a proxy measure of cognitive reserve, intellectual engagement and physical activity across the lifespan, using the LEQ [56]. Higher LEQ was associated with higher LC [^{18}F]FMT Ki_{vis} (beta = 0.33, $p = 0.03$; $n = 46$; Fig. 4). There was no interaction between [^{11}C]PiB and LEQ (beta = −0.26, $p = 0.11$). Parallel analyses substituting raphe [^{18}F]FMT Ki_{vis} found marginal positive relationships with LEQ (dorsal raphe: beta = 0.27, $p = 0.07$; median raphe: beta = 0.28, $p = 0.053$; Fig. S4), and no relationship for midbrain and striatal

Table 1. Relationship between locus coeruleus [^{18}F]FMT Ki_{vis} and [^{18}F] Flortaucipir SUVR.

A. Model (R^2)	Flortaucipir SUVR meta-ROI	Beta	p
1 (0.05)	LC FMT Ki_{vis}	−0.22	0.19
	age	0.27	0.10
	sex	−0.18	0.25
	years education	0.19	0.24
2 (0.21)	LC FMT Ki_{vis}	−0.26	0.08
	PiB status	0.49	**<0.01**
	age	0.15	0.31
	sex	−0.18	0.19
	years education	0.12	0.41
3 (0.44)	LC FMT Ki_{vis}	−0.11	0.40
	PiB status	0.44	**<0.01**
	LC FMT Ki_{vis} *PiB	−0.47	**<0.01**
	age	0.27	**<0.05**
	sex	0.01	0.95
	years education	0.05	0.71
B. Model (R^2)	**Flortaucipir slope meta-ROI**	**Beta**	**p**
1 (0.12)	LC FMT Ki_{vis}	−0.31	0.12
	age	0.30	0.11
	sex	−0.18	0.34
	years education	0.14	0.46
2 (0.29)	LC FMT Ki_{vis}	−0.44	**0.02**
	PiB status	0.44	**0.02**
	age	0.20	0.25
	sex	−0.17	0.29
	years education	0.09	0.61
3 (0.41)	LC FMT Ki_{vis}	−0.11	0.62
	PiB status	0.41	**0.01**
	LC FMT Ki_{vis} *PiB	−0.53	**0.03**
	age	0.49	**0.02**
	sex	0.04	0.81
	years education	−0.04	0.82

(A) There was no overall relationship between locus coeruleus (LC) [^{18}F] FMT Ki_{vis} and [^{18}F]Flortaucipir SUVR. However, there was a significant interaction between [^{18}F]FMT Ki_{vis} and [^{11}C]PiB status such that higher [^{18}F] FMT Ki_{vis} was associated with lower [^{18}F]Flortaucipir SUVR in [^{11}C]PiB positive participants. (B) Higher locus coeruleus (LC) [^{18}F]FMT Ki_{vis} was associated with lower [^{18}F]Flortaucipir SUVR slope for a model including [^{11}C]PiB status as a covariate. Consistent with cross-sectional analyses, there was a significant interaction between [^{18}F]FMT Ki_{vis} and [^{11}C]PiB status. We report standardized beta weights and adjusted R^2. Bolded values indicate significant p-values ($p < 0.05$).

ROIs (midbrain: beta = 0.12, $p = 0.43$; striatum: beta = −0.06, $p = 0.70$; Figure S4). There were no interactions between [^{11}C]PiB and LEQ for raphe and midbrain ROIs (beta = −0.09, $p = 0.57$), but a significant [^{11}C]PiB * LEQ interaction in predicting striatal dopamine synthesis capacity (beta = −0.34, $p = 0.04$). This interaction was driven by [^{11}C]PiB positive individuals who showed higher striatal dopamine synthesis capacity associated with lower LEQ ([^{11}C]PiB positive: $r = -0.59$ [−0.85, −0.08], $p = 0.03$; [^{11}C]PiB negative: $r = 0.10$ [−0.25, 0.43], $p = 0.57$; Fig. S4). The direction of this relationship is opposite to what is observed for LC and raphe ROIs, but is broadly consistent with our previous research suggesting striatal dopamine synthesis is upregulated in aging in the context of brain structural decline [62].

DISCUSSION

This study establishes, for the first time, relationships among PET measures of LC neurochemical function and AD-related pathology, and provides insight into their combined effect on episodic memory performance. These findings suggest [^{18}F]FMT Ki_{vis} is a valuable biomarker of LC neurochemical function and opens up new lines of research examining a protective role of neuromodulator systems in AD and, because the causal directions of these associations are not established, the role of AD pathology in altering LC neurochemistry.

We provide the first in vivo evidence that LC neurochemical function is related to the degree of tau burden and rates of tau accumulation in humans. In older adults with β-amyloid, higher LC catecholamine synthesis capacity was associated with lower temporal lobe tau burden. Further, higher LC catecholamine synthesis capacity was associated with lower rates of tau accumulation over time in a model adjusting for β-amyloid status ($n = 30$). Specifically, lower longitudinal tau slopes were associated with higher LC catecholamine synthesis capacity. These relationships were selective for LC, and were not observed for [^{18}F]FMT signal in the raphe, midbrain, and striatum. The negative association is consistent with two interpretations, which are not mutually exclusive. First, advanced progression of tau pathology may be associated with greater LC tau burden and degeneration, which may reduce neurotransmitter synthesis. Second, higher LC catecholamine synthesis may actively stave off tau's progression via neuroprotective functions [25, 63]. Measurement of tau burden in LC is not possible with available tracers, though longitudinal studies may disambiguate the directionality of these associations.

The neuroprotective functions of norepinephrine [2, 3, 64–68] have inspired proposals that the maintenance of LC neurochemical function confers AD resistance [25, 63], which are supported by demonstrations that the loss of LC-catecholamine signaling increases accumulation of β-amyloid and tau pathology in AD mouse models [21, 22]. However, there is substantial complexity to this line of research, as higher norepinephrine metabolites may promote tau propagation [8], and higher levels of norepinephrine metabolites in AD are associated with greater tau pathology [4, 5]. Norepinephrine metabolites are elevated across the AD spectrum [4, 6, 69], suggesting that there is upregulation of norepinephrine activity in response to disease [69]. It is possible that elevation of norepinephrine activity is desirable, even compensatory, in aging and preclinical AD, but, in later stages, beneficial effects are no longer evident and excessive metabolite generation signals greater disease severity. Additional research is needed to establish how CSF metabolite measures relate to PET measures, and to test the longitudinal trajectories of these measures in preclinical AD and MCI.

Higher LC catecholamine synthesis capacity appeared to mitigate tau's negative effect on memory. The mechanisms by which LC catecholamines enhance memory are well established. The LC projects to the medial temporal lobe [70], and catecholamine release in hippocampus modulates long-term potentiation and depression [71]. In AD mouse models, treatment with a norepinephrine precursor partially restores memory performance despite pathology [72]. Complementing these findings, we found the effect of tau on memory to be reduced in conditions of high catecholamine synthesis. Conferral of better-than-expected cognitive performance given one's pathology burden has been interpreted to reflect resilience [24], and is consistent with proposals that the norepinephrine system is central to mechanisms of reserve in AD [25, 26].

While the norepinephrine system affects cognition [16], cognition likely also affects the norepinephrine system [73, 74]. Specifically, cognitive activity may play a causal role in modifying the LC-norepinephrine system, allowing active older adults to maintain healthy LC-norepinephrine function. In rodent models, experiments manipulating the complexity and novelty of the

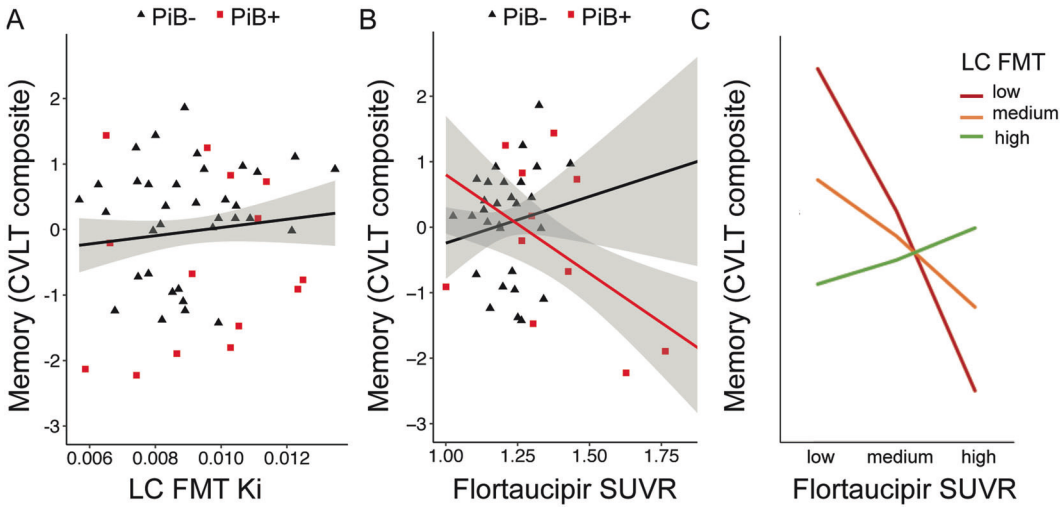

Fig. 3 Associations among locus coeruleus [^{18}F]Fluoro-m-tyrosine (LC [^{18}F]FMT Ki$_{vis}$), memory, and tau. A There was no relationship between LC [^{18}F]FMT Ki$_{vis}$ and memory as measured by the California Verbal Learning Test-II (CVLT) composite. **B** There was a negative relationship between tau burden measured with [^{18}F]Flortaucipir and memory. This relationship was driven by β-amyloid positive participants as defined by [^{11}C]Pittsburgh compound B (PiB). Correlations for [^{11}C]PiB positive and negative participants are displayed separately. **C** There was a significant interaction between LC [^{18}F]FMT Ki$_{vis}$ and [^{18}F]Flortaucipir such that the effect of tau on memory was absent in conditions of high LC [^{18}F]FMT Ki$_{vis}$. We present discrete groupings of the continuous LC [^{18}F]FMT Ki$_{vis}$ variable for display purposes.

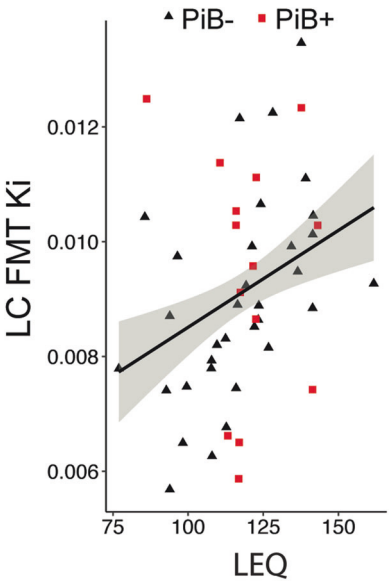

Fig. 4 Lifetime cognitive engagement and [^{18}F]Fluoro-m-tyrosine ([^{18}F]FMT) Ki$_{vis}$. There was a positive relationship between locus coeruleus (LC) [^{18}F]FMT Ki and self-reported cognitive and physical activity across the lifespan as measured by the Lifetime Experiences Questionnaire (LEQ). β-amyloid status as defined by [^{11}C]Pittsburgh compound B (PiB) is identified for individual subjects.

environment find these interventions increase norepinephrine concentration in the brainstem and LC targets [73] and release in hippocampus [74]. As these studies assessed acute effects, the extent to which such enrichment enduringly impacts norepinephrine function, potentially bestowing brain reserve, is unknown. It is important to note that in addition to higher self-reported cognitive and physical activities (LEQ) being associated with higher LC catecholamine synthesis capacity, we found a marginal relationship between higher LEQ and serotonin synthesis capacity in the raphe nuclei, suggesting that the integrity of multiple neuromodulator systems in older age may be associated with lifestyle factors [75].

There are important limitations of this study. It will be critical for future [^{18}F]FMT studies to measure LC-related signal using an arterial plasma input function and pair these measurements with MR perfusion measures to determine the extent to which LC [^{18}F]FMT Ki is affected by blood flow. Additionally, there were relatively few β-amyloid-positive participants. It will be important to replicate our findings in a larger sample. This study was limited by long temporal delays between the acquisition of PET scans. We believe these time differences between scans did not introduce systematic bias as covarying for time did not change our results. Finally, the limited spatial resolution of PET and AADC activity in the raphe nuclei may have reduced our sensitivity for detecting relationships among LC catecholamine function, cognition, and AD-related pathology. Future test-retest reliability assessments for these small structures are needed.

The LC represents a principal site of interactions between neuromodulator systems and AD-related pathology, which are rarely studied in conjunction in humans. Advancing norepinephrine imaging methods promises to inform treatment approaches directly targeting the LC-norepinephrine system [63]. For example, vagal stimulation research developing interventions targeting the LC-norepinephrine system [76–78] would benefit from understanding an individual's baseline LC neurochemical function. The addition of neurochemical imaging tools to complement the rapidly accelerating field of LC biomarker development is a valuable investment given LC's role in basic cognition and the etiology of neurological and psychiatric disorders.

DATA AVAILABILITY

All meta data are available in supplementary information. Access to raw data is contingent on material transfer agreement.

REFERENCES

1. Theofilas P, Dunlop S, Heinsen H, Grinberg LT. Turning on the light within: Subcortical nuclei of the isodentritic core and their role in Alzheimer's disease pathogenesis. J Alzheimers Dis. 2015;46:17–34.
2. Feinstein DL, Heneka MT, Gavrilyuk V, Russo CD, Weinberg G, Galea E. Noradrenergic regulation of inflammatory gene expression in brain. Neurochemistry Int. 2002;41:357–65.

3. Jurič DM, Lončar D, Čarman-Kržan M. Noradrenergic stimulation of BDNF synthesis in astrocytes: Mediation via α1- and β1/β2-adrenergic receptors. Neurochemistry Int. 2008;52:297–306.
4. Jacobs HIL, Riphagen JM, Ramakers IHGB, Verhey FRJ. Alzheimer's disease pathology: Pathways between central norepinephrine activity, memory, and neuropsychiatric symptoms. Mol Psychiatry. 2021;26:897–906.
5. Lawlor BA, Bierer LM, Ryan TM, Schmeidler J, Knott PJ, Williams LL, et al. Plasma 3-methoxy-4-hydroxyphenylglycol (MHPG) and clinical symptoms in Alzheimer's disease. Biol Psychiatry. 1995;38:185–8.
6. Sheline YI, Miller K, Bardgett ME, Csernansky JG. Higher cerebrospinal fluid MHPG in subjects with dementia of the Alzheimer type. Relationship with cognitive dysfunction. Am J Geriatr Psychiatry. 1998;6:155–61.
7. Riphagen JM, van Egroo M, Jacobs HIL. Elevated norepinephrine metabolism gauges Alzheimer's disease-related pathology and memory decline. J Alzheimers Dis. 2021;80:521–6.
8. Kang SS, Liu X, Ahn EH, Xiang J, Manfredsson FP, Yang X, et al. Norepinephrine metabolite DOPEGAL activates AEP and pathological Tau aggregation in locus coeruleus. J Clin Invest. 2020;130:422–37.
9. Betts MJ, Kirilina E, Otaduy MCG, Ivanov D, Acosta-Cabronero J, Callaghan MF, et al. Locus coeruleus imaging as a biomarker for noradrenergic dysfunction in neurodegenerative diseases. Brain. 2019;142:2558–71.
10. Bachman SL, Dahl MJ, Werkle-Bergner M, Düzel S, Forlim CG, Lindenberger U, et al. Locus coeruleus MRI contrast is associated with cortical thickness in older adults. Neurobiol Aging. 2021;100:72–82.
11. Clewett DV, Lee T-H, Greening S, Ponzio A, Margalit E, Mather M. Neuromelanin marks the spot: identifying a locus coeruleus biomarker of cognitive reserve in healthy aging. Neurobiol Aging. 2016;37:117–26.
12. Liu KY, Kievit RA, Tsvetanov KA, Betts MJ, Düzel E, Rowe JB, et al. Noradrenergic-dependent functions are associated with age-related locus coeruleus signal intensity differences. Nat Commun. 2020;11:1712.
13. Betts MJ, Cardenas-Blanco A, Kanowski M, Spottke A, Teipel SJ, Kilimann I, et al. Locus coeruleus MRI contrast is reduced in Alzheimer's disease dementia and correlates with CSF Aβ levels. Alzheimers Dement (Amst). 2019;11:281–5.
14. Jacobs HIL, Becker JA, Kwong K, Engels-Domínguez N, Prokopiou PC, Papp KV, et al. In vivo and neuropathology data support locus coeruleus integrity as indicator of Alzheimer's disease pathology and cognitive decline. Sci Transl Med. 2021;13:eabj2511.
15. Dahl MJ, Mather M, Werkle-Bergner M, Kennedy BL, Qiao Y, Shi Y, et al. Lower MR-indexed locus coeruleus integrity in autosomal-dominant Alzheimer's disease is related to cortical tau burden and memory deficits. MedRxiv. 2020:2020.11.16.20232561.
16. Sara SJ. The locus coeruleus and noradrenergic modulation of cognition. Nat Rev Neurosci. 2009;10:211–23.
17. Mather M, Harley CW. The Locus coeruleus: Essential for maintaining cognitive function and the aging brain. Trends Cogn Sci (Regul Ed). 2016;20:214–26.
18. Dahl MJ, Mather M, Düzel S, Bodammer NC, Lindenberger U, Kühn S, et al. Rostral locus coeruleus integrity is associated with better memory performance in older adults. Nat Hum Behav. 2019;3:1203–14.
19. Hämmerer D, Callaghan MF, Hopkins A, Kosciessa J, Betts M, Cardenas-Blanco A, et al. Locus coeruleus integrity in old age is selectively related to memories linked with salient negative events. Proc Natl Acad Sci USA. 2018;115:2228–33.
20. Langley J, Hussain S, Flores JJ, Bennett IJ, Hu X. Characterization of age-related microstructural changes in locus coeruleus and substantia nigra pars compacta. Neurobiol Aging. 2020;87:89–97.
21. Chalermpalanupap T, Schroeder JP, Rorabaugh JM, Liles LC, Lah JJ, Levey AI, et al. Locus coeruleus ablation exacerbates cognitive deficits, neuropathology, and lethality in P301S tau transgenic mice. J Neurosci. 2018;38:74–92.
22. Heneka MT, Ramanathan M, Jacobs AH, Dumitrescu-Ozimek L, Bilkei-Gorzo A, Debeir T, et al. Locus ceruleus degeneration promotes Alzheimer pathogenesis in amyloid precursor protein 23 transgenic mice. J Neurosci. 2006;26:1343–54.
23. Stern Y, Arenaza-Urquijo EM, Bartrés-Faz D, Belleville S, Cantilon M, Chetelat G, et al. Whitepaper: Defining and investigating cognitive reserve, brain reserve, and brain maintenance. Alzheimers Dement. 2020;16:1305–11.
24. Arenaza-Urquijo EM, Vemuri P. Resistance vs resilience to Alzheimer disease. Neurology. 2018;90:695–703.
25. Robertson IH. A noradrenergic theory of cognitive reserve: Implications for Alzheimer's disease. Neurobiol Aging. 2013;34:298–308.
26. Wilson RS, Boyle PA, Yu L, Barnes LL, Schneider JA, Bennett DA. Life-span cognitive activity, neuropathologic burden, and cognitive aging. Neurology. 2013;81:314–21.
27. Kempadoo KA, Mosharov EV, Choi SJ, Sulzer D, Kandel ER. Dopamine release from the locus coeruleus to the dorsal hippocampus promotes spatial learning and memory. PNAS. 2016;113:14835–40.
28. Berry AS, Shah VD, Baker SL, Vogel JW, O'Neil JP, Janabi M, et al. Aging affects dopaminergic neural mechanisms of cognitive flexibility. J Neurosci. 2016;36:12559–69.
29. VanBrocklin HF, Blagoev M, Hoepping A, O'Neil JP, Klose M, Schubiger PA, et al. A new precursor for the preparation of 6-[18F]-fluoro-L-m-tyrosine (FMT): Efficient synthesis and comparison of radiolabeling. Appl Radiat Isotopes. 2004;61:1289–94.
30. Berry AS, Shah VD, Furman DJ, White RL, Baker SL, O'Neil JP, et al. Dopamine synthesis capacity is associated with D2/3 receptor binding but not dopamine release. Neuropsychopharmacology. 2018;43:1201–11.
31. Patlak CS, Blasberg RG. Graphical evaluation of blood-to-brain transfer constants from multiple-time uptake data. Generalizations. J Cereb Blood Flow Metab. 1985;5:584–90.
32. Ito H, Ota M, Ikoma Y, Seki C, Yasuno F, Takano A. et al. Quantitative analysis of dopamine synthesis in human brain using positron emission tomography with L-[beta-11C]DOPA. Nucl Med Commun. 2006;27:723–31.
33. Keren NI, Lozar CT, Harris KC, Morgan PS, Eckert MA. In vivo mapping of the human locus coeruleus. NeuroImage. 2009;47:1261–7.
34. Betts MJ, Cardenas-Blanco A, Kanowski M, Jessen F, Düzel E. In vivo MRI assessment of the human locus coeruleus along its rostrocaudal extent in young and older adults. Neuroimage. 2017;163:150–9.
35. Tona K-D, Keuken MC, de Rover M, Lakke E, Forstmann BU, Nieuwenhuis S, et al. In vivo visualization of the locus coeruleus in humans: quantifying the test-retest reliability. Brain Struct Funct. 2017;222:4203–17.
36. Ye R, Rua C, O'Callaghan C, Jones PS, Hezemans F, Kaalund SS, et al. An in vivo probabilistic atlas of the human Locus coeruleus at ultra-high field. BioRxiv. 2020:2020.02.03.932087.
37. Doppler CEJ, Kinnerup MB, Brune C, Farrher E, Betts M, Fedorova TD, et al. Regional locus coeruleus degeneration is uncoupled from noradrenergic terminal loss in Parkinson's disease. Brain. 2021:awab236.
38. Sommerauer M, Fedorova TD, Hansen AK, Knudsen K, Otto M, Jeppesen J, et al. Evaluation of the noradrenergic system in Parkinson's disease: an 11C-MeNER PET and neuromelanin MRI study. Brain 2018;141:496–504.
39. Moore RY, Whone AL, Brooks DJ. Extrastriatal monoamine neuron function in Parkinson's disease: An 18F-dopa PET study. Neurobiol Dis. 2008;29:381–90.
40. Pavese N, Rivero-Bosch M, Lewis SJ, Whone AL, Brooks DJ. Progression of monoaminergic dysfunction in Parkinson's disease: a longitudinal 18F-dopa PET study. Neuroimage. 2011;56:1463–8.
41. Remy P, Doder M, Lees A, Turjanski N, Brooks D. Depression in Parkinson's disease: loss of dopamine and noradrenaline innervation in the limbic system. Brain. 2005;128:1314–22.
42. Ding Y-S, Singhal T, Planeta-Wilson B, Gallezot J-D, Nabulsi N, Labaree D, et al. PET imaging of the effects of age and cocaine on the norepinephrine transporter in the human brain using (S,S)-[11C]O-Methylreboxetine and HRRT. Synapse 2010;64:30–8.
43. Ono SA, Sato T, Muramatsu S. Freezing of gait in Parkinson's disease is associated with reduced 6-[18F]Fluoro-l-m-tyrosine uptake in the locus coeruleus. Parkinsons Dis. 2016;2016:5430920.
44. Brumberg J, Tran-Gia J, Lapa C, Isaias IU, Samnick S. PET imaging of noradrenaline transporters in Parkinson's disease: Focus on scan time. Ann Nucl Med. 2019;33:69–77.
45. Coull JT, Büchel C, Friston KJ, Frith CD. Noradrenergically mediated plasticity in a human attentional neuronal network. NeuroImage. 1999;10:705–15.
46. Labus J, Naliboff B, Fallon J, Berman S, Suyenobu B, Bueller J, et al. Sex differences in brain activity during aversive visceral stimulation and its expectation in patients with chronic abdominal pain: A network analysis. Neuroimage. 2008;41:1032–43.
47. Liu KY, Acosta-Cabronero J, Hong YT, Yi Y-J, Hämmerer D, Howard R. FDG-PET assessment of the locus coeruleus in Alzheimer's disease. Neuroimage: Rep. 2021;1:100002.
48. Schöll M, Lockhart SN, Schonhaut DR, O'Neil JP, Janabi M, Ossenkoppele R, et al. PET Imaging of Tau deposition in the aging human brain. Neuron. 2016;89:971–82.
49. Price JC, Klunk WE, Lopresti BJ, Lu X, Hoge JA, Ziolko SK, et al. Kinetic modeling of amyloid binding in humans using PET imaging and Pittsburgh Compound-B. J Cereb Blood Flow Metab. 2005;25:1528–47.
50. Villeneuve S, Rabinovici GD, Cohn-Sheehy BI, Madison C, Ayakta N, Ghosh PM, et al. Existing Pittsburgh Compound-B positron emission tomography thresholds are too high: statistical and pathological evaluation. Brain. 2015;138:2020–33.
51. Mormino EC, Brandel MG, Madison CM, Rabinovici GD, Marks S, Baker SL, et al. Not quite PIB-positive, not quite PIB-negative: Slight PIB elevations in elderly normal control subjects are biologically relevant. Neuroimage. 2012;59:1152–60.
52. Baker SL, Maass A, Jagust WJ. Considerations and code for partial volume correcting [18F]-AV-1451 tau PET data. Data Brief. 2017;15:648–57.

53. Jack CR, Wiste HJ, Weigand SD, Therneau TM, Lowe VJ, Knopman DS, et al. Defining imaging biomarker cut points for brain aging and Alzheimer's disease. Alzheimers Dement. 2017;13:205–16.
54. Harrison TM, La Joie R, Maass A, Baker SL, Swinnerton K, Fenton L, et al. Longitudinal tau accumulation and atrophy in aging and alzheimer disease. Ann Neurol. 2019;85:229–40.
55. Woods SP, Delis DC, Scott JC, Kramer JH, Holdnack JA. The California verbal learning test—second edition: Test-retest reliability, practice effects, and reliable change indices for the standard and alternate forms. Arch Clin Neuropsychol. 2006;21:413–20.
56. Valenzuela MJ, Sachdev P. Assessment of complex mental activity across the lifespan: development of the Lifetime of Experiences Questionnaire (LEQ). Psychol Med. 2007;37:1015–25.
57. Braak H, Thal DR, Ghebremedhin E, Del Tredici K. Stages of the pathologic process in Alzheimer disease: age categories from 1 to 100 years. J Neuropathol Exp Neurol 2011;70:960–9.
58. Shin RW, Kitamoto T, Tateishi J. Modified tau is present in younger nondemented persons: A study of subcortical nuclei in Alzheimer's disease and progressive supranuclear palsy. Acta Neuropathol. 1991;81:517–23.
59. Pernet CR, Wilcox R, Rousselet GA. Robust correlation analyses: False positive and power validation using a new open source matlab toolbox. Front Psychol. 2012;3:606.
60. Hayes AF. Introduction to mediation, moderation, and conditional process analysis: A regression-based approach. New York: Gilford press; 2013.
61. Maass A, Lockhart SN, Harrison TM, Bell RK, Mellinger T, Swinnerton K, et al. Entorhinal Tau pathology, episodic memory decline, and neurodegeneration in aging. J Neurosci 2018;38:530–43.
62. Ciampa CJ, Parent JH, Lapoint MR, Swinnerton KN, Taylor MM, Tennant VR, et al. Elevated dopamine synthesis as a mechanism of cognitive resilience in aging. Cereb Cortex. 2021:bhab379.
63. Matchett BJ, Grinberg LT, Theofilas P, Murray ME. The mechanistic link between selective vulnerability of the locus coeruleus and neurodegeneration in Alzheimer's disease. Acta Neuropathol. 2021. 11 January 2021. https://doi.org/10.1007/s00401-020-02248-1.
64. Harik SI, McGunigal T. The protective influence of the locus ceruleus on the blood-brain barrier. Ann Neurol. 1984;15:568–74.
65. Ouyang M, Hellman K, Abel T, Thomas SA. Adrenergic signaling plays a critical role in the maintenance of waking and in the regulation of REM sleep. J Neurophysiol. 2004;92:2071–82.
66. Kong Y, Ruan L, Qian L, Liu X, Le Y. Norepinephrine promotes microglia to uptake and degrade amyloid beta peptide through upregulation of mouse formyl peptide receptor 2 and induction of insulin-degrading enzyme. J Neurosci. 2010;30:11848–57.
67. Troadec JD, Marien M, Darios F, Hartmann A, Ruberg M, Colpaert F, et al. Noradrenaline provides long-term protection to dopaminergic neurons by reducing oxidative stress. J Neurochem. 2001;79:200–10.
68. Madrigal JLM, Leza JC, Polak P, Kalinin S, Feinstein DL. Astrocyte-derived MCP-1 mediates neuroprotective effects of noradrenaline. J Neurosci. 2009;29:263–7.
69. Hoogendijk WJG, Feenstra MGP, Botterblom MHA, Gilhuis J, Sommer IEC, Kamphorst W, et al. Increased activity of surviving locus ceruleus neurons in Alzheimer's disease. Ann Neurol. 1999;45:82–91.
70. Jh F, Da K, Ry M. Catecholamine Innervation of the Basal Forebrain. Ii. Amygdala, Suprarhinal Cortex and Entorhinal Cortex. J Comparative Neurol. 1978. http://pubmed.ncbi.nlm.nih.gov/659673/. Accessed 10 June 2020.
71. Hansen N. The longevity of Hippocampus-dependent memory is orchestrated by the Locus Coeruleus-noradrenergic system. Neural Plast. 2017;2017:2727602.
72. Hammerschmidt T, Kummer MP, Terwel D, Martinez A, Gorji A, Pape H-C, et al. Selective loss of noradrenaline exacerbates early cognitive dysfunction and synaptic deficits in APP/PS1 mice. Biol Psychiatry. 2013;73:454–63.
73. Naka F, Shiga T, Yaguchi M, Okado N. An enriched environment increases noradrenaline concentration in the mouse brain. Brain Res. 2002;924:124–6.
74. Grilli M, Zappettini S, Zanardi A, Lagomarsino F, Pittaluga A, Zoli M, et al. Exposure to an enriched environment selectively increases the functional response of the pre-synaptic NMDA receptors which modulate noradrenaline release in mouse hippocampus. J Neurochem. 2009;110:1598–606.
75. Salmon P. Effects of physical exercise on anxiety, depression, and sensitivity to stress: A unifying theory. Clin Psychol Rev. 2001;21:33–61.
76. Farmer AD, Strzelczyk A, Finisguerra A, Gourine AV, Gharabaghi A, Hasan A, et al. International consensus based review and recommendations for minimum reporting standards in research on transcutaneous Vagus Nerve Stimulation (Version 2020). Front Hum Neurosci. 2020;14:409.
77. Sharon O, Fahoum F, Nir Y. Transcutaneous vagus nerve stimulation in humans induces pupil dilation and attenuates alpha oscillations. J Neurosci. 2021;41:320–30.
78. Chang C-H, Lane H-Y, Lin C-H. Brain stimulation in Alzheimer's disease. Front Psychiatry. 2018;9:201.

ACKNOWLEDGEMENTS

Avid Radiopharmaceuticals enabled the use of the [^{18}F]Flortaucipir tracer, but did not provide direct funding and were not involved in data analysis or interpretation. MR data were collected at the Henry H. Wheeler, Jr. Brain Imaging Center, which receives support from the National Science Foundation through their Major Research Instrumentation Program, award number BCS-0821855. We thank Renaud La Joie and Leonardo Iaccarino for helpful discussions, and Michael Sommerauer for generously sharing raphe nuclei regions of interest.

AUTHOR CONTRIBUTIONS

ASB, WJJ, MD, MJB, AM, and JRW conceived of the analyses. ASB, WJJ, MJ, and DF collected data. ASB, CJC, JHP, TMH, RMF, and SLB analyzed the data. ASB, CJC, and JHP wrote the paper with input from all authors.

FUNDING

This research was supported by the following grants: National Institute of Heath grant AG058748 (ASB), AG072328 (ASB), AG034570 (WJJ), AG062542 (WJJ), AG044292 (WJJ), DA034685 (MD), F31AG063428 (JRW), Alzheimer's Association Award AARF-17-530186 (ASB), Deutsche Forschungsgemeinschaft (DFG, German Research Foundation) – Project-ID 425899996 – SFB 1436 (MB). All other authors have no financial disclosures.

CONFLICT OF INTEREST

Dr. Jagust has served as a consultant to Biogen, and Bioclinica, Roche/Genentech, Grifols and holds an equity interest in Optoceutics.

ADDITIONAL INFORMATION

Supplementary information The online version contains supplementary material available at https://doi.org/10.1038/s41386-022-01269-6.

Correspondence and requests for materials should be addressed to Anne S. Berry.

Reprints and permission information is available at http://www.nature.com/reprints

Publisher's note Springer Nature remains neutral with regard to jurisdictional claims in published maps and institutional affiliations.